Article:

Thermal Modelling of Hollow Conductors for Direct Cooling of Electrical Machines

X. Chen, Member, IEEE, J. Wang, Senior Member, IEEE, A. Griffo, Member, IEEE, and A. Spagnolo

Abstract—A direct cooling design using hollow conductors with the coolant flowing inside can significantly improve the heat dissipation in an electrical machine. To predict the thermal performances of an electrical machine with such cooling configuration, this paper proposes a computationally efficient thermal model of hollow conductors with direct cooling features. The hollow conductor is modelled using four equivalent solid cuboidal elements with a three dimensional thermal network and internal heat generation. The heat transfer coefficient between the coolant and conductors is determined by an empirical model considering fluid dynamics behaviors. Axial discretization is performed to take into account the non-uniform temperature distribution along the axial direction. Experimental validation is performed with a U-shaped hollow conductor test rig. Compared to computational fluid dynamics analysis, the proposed thermal model is much more computationally efficient, and thus can be incorporated into design optimization process and electro-thermal simulations of the electrical machine over a driving cycle.

Index Terms—Thermal model, hollow conductor, direct cooling, electrical machine.

I. INTRODUCTION

Power losses produced in an electrical machine result in temperature rise in its internal components. Electrical performances and the maximum machine temperatures largely depend on the amount of the heat that the cooling system can effectively remove. Thermal management and heat extraction systems in automotive traction machines have been extensively reviewed in [1, 2]. Although some innovative solutions using novel materials e.g. graphite sheets [3] and thermomagnetic liquids [4] have been proposed, the vast majority of cooling systems in traction machines use direct or indirect liquid cooling of stator windings using oil [5] or a mixture of water-glycol. Compared to air cooling systems [6, 7], a liquid cooling system [8, 9] typically is more complex but results in smaller size, less weight and higher heat transfer rate. In a conventional liquid cooled machine, the stator outer bore is enclosed by a cooling jacket which removes the heat from the active parts of the electrical machine and dissipates it to ambient. However, the heat generated in the windings has to flow through wire insulation, impregnation, slot liner, stator tooth and back-iron, interface gap between stator outer bore and cooling jacket, and cooling jacket wall, before being dissipated to the coolant [10]. Hence, to shorten this heat flow path and reduce the total thermal resistance, direct cooling of the internal components of an electrical machine has been proposed in [11-19]. In [11, 12], a spraying technique was utilized to assist the cooling of end-windings while the active part was still cooled by conventional cooling jacket. A permanent magnet starter-generator with flooded-stator cooling configuration was developed in [13, 14]. A sleeve attached to the stator inner bore was employed to avoid the coolant penetrating into the rotor region. The coolant flows axially via ducts in both slot-openings and stator back-iron to carry the heat flow. An interior permanent magnet machine with axial cooling ducts on stator back-iron was proposed in [15], demonstrating improved cooling performances of the direct cooling configuration. A yokeless and segmented armature axial flux machine with flooded-stator cooling design was proposed in [16, 17]. Due to its yokeless segmented armature topology, the coolant flows in both the radial and circumferential directions and thus has a large heat transfer area. An axial flux permanent magnet machine with directly cooled hollow conductors, with coolant flow in the axial direction, was proposed in [18, 19]. Although these direct cooling techniques improve the machine thermal performances, they complicate the manufacture and assembly, resulting in higher cost. Hence, they can only be justified in the applications with very demanding thermal requirements.

To evaluate the benefits and optimize the design of such electrical machines with direct cooling systems an accurate thermal model is essential. Most thermal modelling techniques for directly cooled electrical machines available in literature are based on computational fluid dynamics (CFD) simulations, such as [13-15, 17-19]. A lumped parameter thermal model was proposed in [16], for a yokeless and segmented armature axial flux machine with flooded-stator cooling configuration. The heat transfer coefficient between the coolant and windings was predicted based on the flow distribution determined by the fluid

X. Chen, J. Wang and A. Griffo are with the Department of Electronic and Electrical Engineering, The University of Sheffield, Sheffield S1 3JD, United Kingdom, (e-mail: x.chen.1988@ieee.org; j.b.wang@sheffield.ac.uk; a.griffo@sheffield.ac.uk).
A. Spagnolo is with Research In Energy and Electronics, Siemens AG, Erlangen 91058, Germany (e-mail: aristide.spagnolo@siemens.com).

model. Although CFD models can be accurate and offer more insights in the fluid dynamics behaviors, their computational time and efforts are much higher than lumped parameter thermal models [20].

To minimize the thermal resistance between the winding and the coolant, thus enhancing the electrical machine cooling performance and improving the torque density, a number of direct winding cooling solutions have been proposed. Reference [5] describes an effective solution using oil-spray cooling on the end windings. However the need for spraying nozzles in the housing reduces the practicality of the proposal. Cooling channels inserted in the slots in direct contact with the windings have been proposed [21, 22]. Again, despite the thermal benefits, complexity of manufacturing and reduced fill factor might reduce the appeal of these solutions. A simpler method based on the insertion of a silicon pipe in direct contact with the end-windings has been proposed in [23].

This paper investigates hollow conductor windings with direct cooling. The use of directly cooled hollow conductors can achieve significant improvements in heat removal without significantly affecting manufacturing and slot fill factor. As illustrated in Fig. 1, the heat generated in the winding hollow conductor can be directly dissipated to the circulating coolant inside the conductor, leading to significantly improved cooling performance. To effectively design a machine with such a cooling scheme, an accurate and computationally efficient thermal model is essential. However, no lumped parameter thermal model in such applications has been reported in literature although an analytical thermal model of a generic cuboidal element was proposed in [24]. To address the problem, this paper proposes a computationally efficient thermal model of hollow conductors with direct cooling features, considering the non-uniform temperature distributions over various conductor walls, the fluid dynamics and the enthalpy carried by the coolant. Experimental validation is performed with a U-shaped hollow conductor test rig. The developed model is employed to design a high power interior permanent magnet (IPM) machine for electric vehicle applications. Furthermore, a 62.7kW IPM machine with both direct cooling features and conventional liquid cooling jackets is prototyped, and the comparison of these two cooling schemes are performed to demonstrate the advantages of the direct cooling configuration with hollow conductors.

The main contributions of the paper are as follows. First a thermal model for machine windings employing hollow conductors with direct cooling has been developed. Compared to computational fluid dynamics analysis, the proposed thermal model is much more computationally efficient, and thus can be incorporated into design optimization process or in electro-thermal simulations of the electrical machine over a mission profile. Further the proposed thermal model has been incorporated into the thermal analysis of an electrical machine with direct cooling. The validity of the model and the benefits of the direct cooling have been demonstrated experimentally. These would facilitate further improvements in machine torque density and efficiency, which are crucial in a variety of applications.

II. THERMAL MODEL OF HOLLOW CUBOIDAL ELEMENT

This section describes the proposed thermal model of a hollow cuboidal element with direct cooling features, including the thermal models of the hollow conductor and the internal coolant.

A. Thermal Model of Hollow Conductor

The hollow cuboidal element shown in Fig. 1 can be split into 4 solid trapezoidal elements along the diagonal lines (blue dashed lines in Fig. 1). Each solid trapezoidal element can be simplified to an equivalent solid cuboidal element with its inner surface connecting to the coolant node through a convection resistance, as illustrated in Fig. 2.
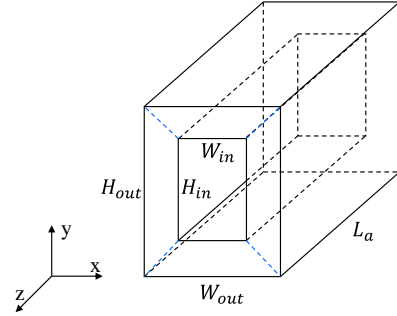
Fig. 1. Geometry of a hollow cuboidal element.
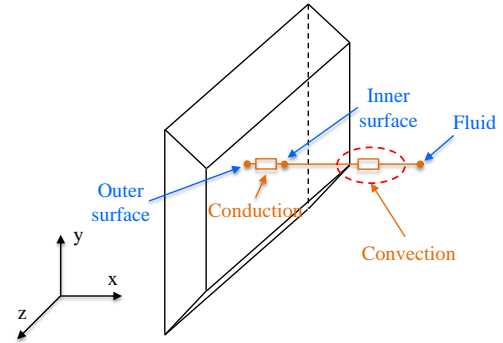
Fig. 2. Thermal network of one quarter hollow cuboidal element along the primary thermal dissipation direction.

An axial segment of the hollow conductor is then represented by 4 equivalent solid cuboidal elements with their inner surfaces connecting to the coolant node through equivalent thermal resistances. Fig. 3 shows the thermal model of the solid cuboidal element. $R_{x1} + R_{x2}$ is the thermal resistance in the x direction, R_{x3} is a compensating thermal resistance to correctly predict the average cuboidal temperature $\bar{T}$. T_{x1} and T_{x2} represent the temperatures of the two outer surfaces perpendicular to the x axis. The thermal resistances and temperatures in y and z directions also follow the same convention. C and $\dot{q}$ are the heat capacity and internal heat power, respectively.

A merit of this model is that it can accurately predict the average temperature of a solid cuboidal element with internal heat generation, by introducing an equivalent thermal node $\bar{T}$.
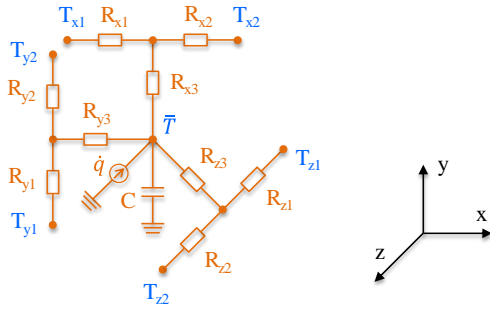
Fig. 3. Schematic of the solid cuboidal element thermal model from [24].

Fig. 4 depicts the thermal network of the proposed hollow cuboidal element with internal liquid cooling. R_{fi} (i=1, 2, 3, 4) represents the equivalent thermal resistance between the ith solid cuboidal element inner surface and the coolant node. T_f is the coolant temperature. The first digits of the subscripts of the thermal resistances, heat capacities, and internal heat powers represent the quantities for the ith solid cuboidal element. The connections between T_{x31} and T_{y12}, between T_{y11} and T_{x41}, between T_{x42} and T_{y21}, and between T_{y22} and T_{x32} represent the physical connections of the 4 solid cuboidal elements.

The thermal resistances R_{xi1}, R_{xi2}, R_{yi1}, R_{yi2}, R_{zi1} and R_{zi2} are determined based on the one-dimensional steady-state heat diffusion equation with zero internal heat generation condition. The trapezoidal cross section of each solid cuboid element is simplified to a rectangle shape with equivalent area as shown in Fig. 5.

Thus, the thermal resistances R_{xi1} and R_{xi2} shown in Fig. 4 can be calculated using (1), assuming they are symmetric.

$$R_{xi1} = R_{xi2} = \frac{l_{xi}}{2k_x A_{xi}} \tag{1}$$

where k_x is the x-axis thermal conductivity of the conductor,

l_{xi} is the x-axis dimension of the ith solid cuboidal element as shown in Fig. 5, A_{xi} is the area of the equivalent i[th] solid cuboidal element surface which is perpendicular to x axis and are given by:

$$A_{x1} = A_{x2} = \frac{H_{in} + H_{out}}{2} L_a \tag{2}$$

$$A_{x3} = A_{x4} = \frac{H_{out} - H_{in}}{2} L_a \tag{3}$$

where H_{out} and H_{in} are the heights of the outer and inner cross sections of the hollow conductor, respectively, and L_a is the axial length of the hollow conductor, as illustrated in Fig. 1.

The thermal resistances R_{yi1} and R_{yi2} and R_{zi1} and R_{zi2} are calculated similarly. R_{xi3}, R_{yi3}, and R_{zi3} are the dummy thermal resistances introduced in order to predict the average temperature of the ith equivalent solid cuboidal element [24]. They can be determined based on the superposition of the one-dimensional steady-state heat diffusion equation with zero internal heat generation condition and that with zero surface temperature boundary conditions. Therefore, the equivalent thermal resistance R_{xi3} in Fig. 4 is calculated by:

$$R_{xi3} = -\frac{l_{xi}}{6k_x A_{xi}} \tag{4}$$

R_{yij} and R_{zij} can be calculated in a similar way and l_{yi}, A_{yi}, l_{zi} and A_{zi} need to be specified accordingly. $\dot{q}_i$ and C_i in Fig. 4 are the internal heat power and heat capacity of the ith equivalent solid cuboidal element, respectively. C_i can be calculated by:

$$C_i = c_p \rho V_i \tag{5}$$

where c_p and ρ are the specific heat capacity and density of the conductor material, respectively, and V_i is volume of the ith equivalent solid cuboidal element.
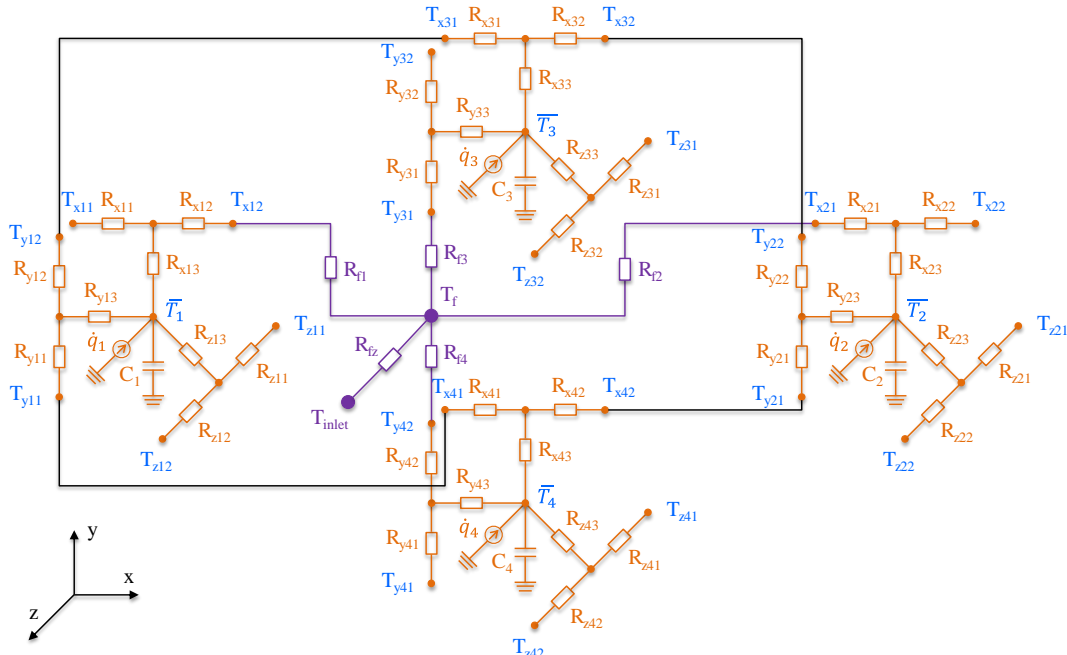
Fig. 4. Thermal network of the proposed hollow cuboidal element.
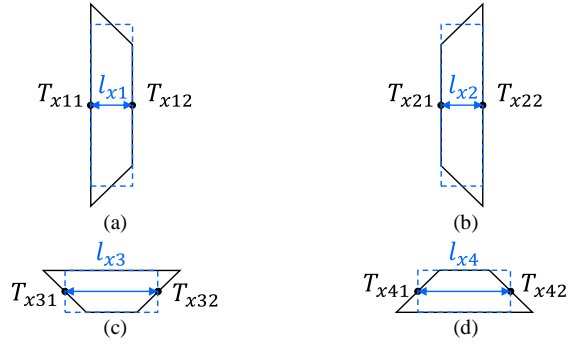
Fig. 5. Four equivalent cuboidal elements with x-axis thermal dimensions. (a) First element. (b) Second element. (c) Third element. (d) Fourth element.

B. Thermal Model of Internal Coolant

The coolant inside the hollow conductor is modeled as a thermal mass connected to the internal surfaces of the hollow conductor through equivalent thermal resistances. As shown in Fig. 4, the thermal resistance R_{fi} represents the internal forced convection applied to the ith equivalent solid cuboidal element of the hollow conductor. R_{fz} is the equivalent thermal resistance to take into account the enthalpy carried by coolant in the flow direction (z-axis in this paper). To calculate R_{fi} and R_{fz}, the following steps need to be performed.

The hydraulic diameter D_h is defined by (6).

$$D_h = \frac{4A_c}{per} \tag{6}$$

where A_c is the area of the internal hollow duct and can be calculated using $H_{in}W_{in}$. per is the wetted perimeter of the internal hollow duct and can be predicted by (7), given that the duct cross section is a rectangular shape.

$$per = 2(H_{in}+W_{in}) \tag{7}$$

The Reynolds number can be calculated by:

$$Re = \frac{\rho_f D_h u_f}{\mu_f} \tag{8}$$

where ρ_f is the density of the coolant, μ_f is the dynamic viscosity of the coolant, and u_f is the mean velocity of the coolant:

$$u_f = \frac{\dot{V}}{A_c} \tag{9}$$

where $\dot{V}$ is the mean volumetric flow rate of the coolant in m³/s. If the calculated Reynolds number $Re < 2300$, the flow will be laminar. Otherwise, it will be turbulent or a combination of both turbulent and laminar flow. In this application, the duct size is 3mm×1mm, and the volumetric flow rate is lower than 0.052L/min (the flow rate of all the 192 conductors in the complete electrical machine is no higher than 10L/min). Therefore, the Reynolds number Re is much less than 2300 resulting in laminar flow. The equations presented below are valid for laminar flow only. The hydraulic and thermal entry lengths for a laminar flow can be estimated by (10) and (11) [25], respectively.

$$L_{entry\_h} \approx 0.06 Re D_h \tag{10}$$
$$L_{entry\_t} \approx 0.06 Re D_h Pr_f \tag{11}$$

where Pr_f is Prandtl number which is defined by (12).

$$Pr_f = \frac{v_f}{\alpha_f} \tag{12}$$

where v_f is the kinematic viscosity of the coolant and is defined as the ratio of the coolant dynamic viscosity to its density, i.e. μ_f/ρ_f. α_f is the thermal diffusivity of the coolant.

In this application, Fragoltherm X80 is employed as the coolant medium considering its good thermal and fluidic properties for the proposed cooling scheme, and the estimated Pr_f is approximately 110. The predicted hydraulic entry length L_{entry_h} and thermal entry length L_{entry_t} are approximately 4.6mm and 506mm, respectively. They are approximately 2.3% and 253% of the 200mm axial active length of the hollow conductor, respectively. Therefore, the flow character in this application is hydrodynamically developed and thermally developing laminar flow. In these conditions, the mean Nusselt number Nu can be predicted by (13) based on the experimental data published by P. Wibulswas in [26].

$$Nu = f(Gz, AR) \tag{13}$$

where Gz is the Graetz number as defined in (14), and AR is the duct aspect ratio defined as the ratio of the maximum to the minimum dimensions of the duct as described in (15).

$$Gz = \frac{D_h Re Pr_{\_f}}{L_a} \tag{14}$$
$$AR = max\left\{\frac{W_{in}}{H_{in}}, \frac{H_{in}}{W_{in}}\right\} \tag{15}$$

The convective heat transfer coefficient h_f between the coolant and the hollow conductor inner surfaces is given by:

$$h_f = \frac{k_f Nu}{D_h} \tag{16}$$

where k_f is the thermal conductivity of the coolant. Finally, the equivalent thermal resistances R_{fi} can be predicted using:

$$R_{f1} = R_{f2} = \frac{1}{h_f H_{in} L_a} \tag{17}$$
$$R_{f3} = R_{f4} = \frac{1}{h_f W_{in} L_a} \tag{18}$$

In general, the energy balance equation in a medium inside a channel with forced convection contains terms representing the heat transfer from the duct wall to the coolant; the volumetric generation due to viscous dissipation; externally imposed volumetric generation in the coolant; enthalpy carried by the coolant; and axial conduction in the coolant. However, in most cases, the dominated energy components are only the heat transfer from the duct wall to the coolant and the enthalpy carried by the coolant, as described by:

$$\dot{q}_s'' per = \dot{m}_f c_{p\_f} \frac{dT_f}{dz} \tag{19}$$

where $\dot{q}_s''$ is the heat power density per unit area from the duct wall to coolant, per is the wetted perimeter of the internal hollow duct and can be predicted by (7), $\dot{m}_f$ is the coolant mass flow rate, c_{p_f} is the specific heat capacity of the coolant, T_f is the coolant mean temperature (over its cross-section) which varies with the variation of axial location z. Based on (19), the coolant mean temperature T_f can be derived as:

$$T_f(z) = T_{inlet} + \frac{\dot{q}_s}{\dot{m}_f c_{p\_f}} \cdot \frac{z}{L_a} \tag{20}$$

where $\dot{q}_s$ is the heat power transferred from the duct wall to the coolant. Considering the continuity of the heat power, the equivalent heat power carried by the coolant satisfies $\dot{q}_f = \dot{q}_s$. Thus, the equivalent thermal resistance R_{fz} is:

$$R_{fz}(z) = \frac{T_f(z) - T_{inlet}}{\dot{q}_f} = \frac{z}{\dot{m}_f c_{p\_f} L_a} \tag{21}$$

Due to the fact that R_{fz} varies with z, the average R_{fz} over z can be used in the simulation if only one thermal node in the axial direction is employed. Thus, R_{fz} can be simplified to:

$$R_{fz} = \frac{1}{2\dot{m}_f c_{p\_f}} \tag{22}$$

It should be noted that (22) cannot capture the coolant temperature distribution over the axial direction. To improve the model accuracy, an axial discretization with a certain number of elements is recommended. Then, the equivalent thermal resistance between two neighboring coolant elements of the jth pair to take into account the enthalpy carried by coolant in the flow direction can be calculated using:

$$R_{fz\_j} = \frac{\Delta z_j}{\dot{m}_f c_{p\_f} L_a} \tag{23}$$

where Δz_j is the axial distance between two neighboring thermal nodes of the jth pair. This discretization will be discussed in Section III.B.

III. RESULTS

A. Experimental Setup

To validate the proposed thermal model, a hollow conductor has been prototyped, as illustrated in Fig. 6.
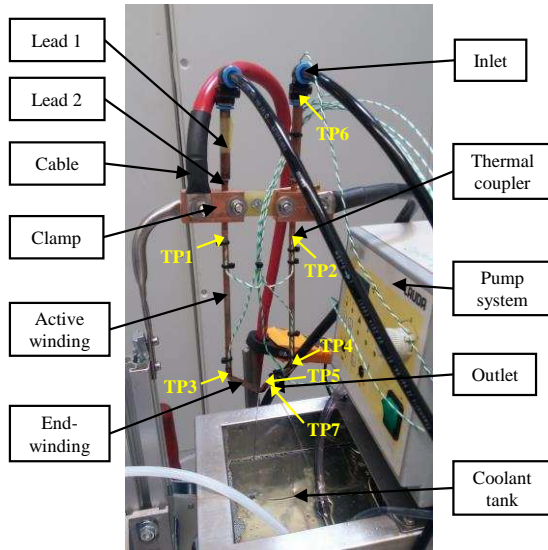
Fig. 6. Experimental setup.

It can be seen that the experimental setup includes a vertically placed hollow conductor consisting of both active winding and end-winding region. A DC power source feeds electric current into the hollow conductor through the cable and clamp. The coolant is fed to the inlets of the two hollow conductor sides before returning to the coolant tank via the outlet. Seven temperature sensors, whose locations are listed in Table I, are employed, as shown in Fig. 6.

The dimensions of the conductor prototype and experimental setup are illustrated in Fig. 7.

TABLE I
TEMPERATURE SENSOR LOCATIONS

Temperature sensor	Location
TP1	Active winding - front
TP2	Active winding - front
TP3	Active winding - rear
TP4	Active winding - rear
TP5	End-winding - rear
TP6	Coolant - inlet
TP7	Coolant - outlet
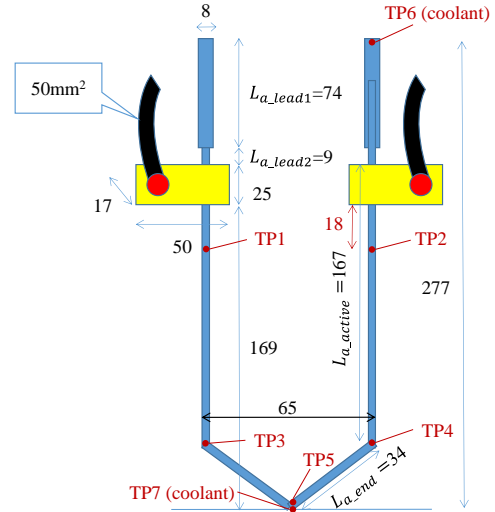
Fig. 7. Dimensions of the experimental setup (dimensions in mm).

It should be noted that in an electrical machine, the hollow conductor is located in a slot and thus exchanges heat with its surroundings by conduction. However, in this experiment, the hollow conductor is exposed to air, and therefore the natural convection and radiation to air need to be modeled. These two mechanisms are described in Section III.C.

B. Thermal Model

To perform comparison with experimental results, a model is proposed, as shown in Fig. 8. Each block (except for the 'clamp' block) is a hollow cuboidal element shown in Fig. 4. The active winding and end-winding are discretized into 4 and 2 elements, respectively. The purple lines represent the coolant circuit, while the orange lines are the physical connections between conductor elements. R_{fz_j} can be calculated using (23). Table II lists the dimensions of the hollow conductor, and L_{a_active}, L_{a_end}, L_{a_lead1} and L_{a_lead2} are illustrated in Fig. 7. It should be noted that the internal heat power only applies to the clamp, active winding and end-winding blocks. The natural convection and radiation are also considered in all the blocks in Fig. 8. With the model in Fig. 8, the axial distribution of the coolant and conductor temperature can be more accurately predicted.

TABLE II
DIMENSIONS OF THE HOLLOW CONDUCTOR

Parameter	Unit	Value
H_{out}	mm	3
H_{in}	mm	1
W_{out}	mm	5
W_{in}	mm	3
L_{a_active}	mm	167
L_{a_end}	mm	34
L_{a_lead1}	mm	74
L_{a_lead2}	mm	9
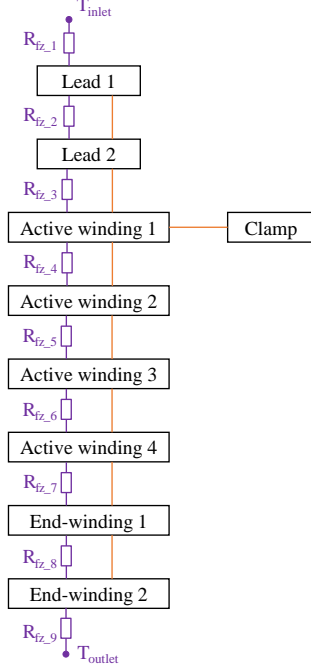
Fig. 8. Equivalent thermal model of the experimental setup.

C. Natural Convection and Radiation

Due to the fact that the hollow conductor is exposed to air in the experiments, this section describes the natural convection and radiation models used in the simulation before comparing with the measured thermal results. The hollow conductor is treated as a vertical plate, neglecting the tilt angle of the end-winding. The Rayleigh number Ra_{air} can be calculated using:

$$Ra_{air} = \frac{g L_a{}^3 \beta (T_{si} - T_{amb})}{\nu_{air} \alpha_{air}} \quad (24)$$

where g is the gravitational acceleration, β is the air volumetric thermal expansion coefficient which can be calculated by the reciprocal of its absolute temperature, T_{si} is the outer surface temperature of the ith equivalent solid cuboidal element, T_{amb} is the ambient air temperature, ν_{air} is the air kinematic viscosity, and α_{air} is the air thermal diffusivity.

The average Nusselt number Nu_{air} is calculated by asymptotically weighting the Nusselt numbers for laminar and turbulent flow using the empirical formula (25) [25].

$$Nu_{air} = \left(Nu_{air\_lam}{}^6 + Nu_{air\_turb}{}^6 \right)^{\frac{1}{6}} \quad (25)$$

where the laminar Nusselt number Nu_{air_lam} and turbulent Nusselt number Nu_{air_turb} can be estimated by (26) and (27)

[25], respectively.

$$Nu_{air\_lam} = \frac{2.0}{\ln\left(1 + \frac{2.0}{C_{lam} Ra_{air}{}^{0.25}}\right)} \quad (26)$$

$$Nu_{air\_turb} = \frac{C_{turb} Ra_{air}{}^{1/3}}{1 + \frac{Pr_{air}}{Ra_{air}} \cdot 1.4 \times 10^9} \quad (27)$$

where Pr_{air} is the Prandtl number of the air, C_{lam} and C_{turb} can be calculated by (28) and (29) [25] respectively.

$$C_{lam} = \frac{0.671}{\left[1 + \left(\frac{0.492}{Pr_{air}}\right)^{9/16}\right]^{4/9}} \quad (28)$$

$$C_{turb} = \frac{0.13 Pr_{air}{}^{0.22}}{\left(1 + 0.61 Pr_{air}{}^{0.81}\right)^{0.42}} \quad (29)$$

Then, the convective heat transfer coefficient h_{air} between the outer surfaces of the hollow conductor and the ambient air can be calculated using:

$$h_{air} = \frac{k_{air} Nu_{air}}{L_a} \quad (30)$$

where k_{air} is the air thermal conductivity. The equivalent thermal resistance R_{air_i} representing the natural convection between the outer surface of the ith equivalent solid cuboidal element and the ambient air can be predicted using (31) and (32).

$$R_{air\_1} = R_{air\_2} = \frac{1}{h_{air} H_{out} L_a} \quad (31)$$

$$R_{air\_3} = R_{air\_4} = \frac{1}{h_{air} W_{out} L_a} \quad (32)$$

The radiative heat transfer coefficient h_{rad} between the outer surface of the ith equivalent solid cuboidal element and the ambient air can be calculated by:

$$h_{rad\_i} = \varepsilon \sigma (T_{si}{}^2 + T_{amb}{}^2)(T_{si} + T_{amb}) \quad (33)$$

where ε is the emissivity of the hollow conductor surface, and σ is Boltzmann constant. The equivalent thermal resistance R_{rad_i} representing the radiation heat transfer between the outer surface of the ith equivalent solid cuboidal element and the ambient air can be predicted as:

$$R_{rad\_1} = R_{rad\_2} = \frac{1}{h_{rad\_1} H_{out} L_a} \quad (34)$$

$$R_{rad\_3} = R_{rad\_4} = \frac{1}{h_{rad\_3} W_{out} L_a} \quad (35)$$

D. Experimental Validation

With the natural convection and radiation effects described in Section III.C incorporated into the discretized thermal model shown in Fig. 8, this section compares the model-predicted thermal results with the measurements. The thermal performances of the hollow conductor are measured at various load conditions, including 100A, 250A and 400A DC currents with 0.067L/min, 0.11L/min and 0.154L/min coolant volumetric flow rate, respectively. The resulting current densities are 8.3A/mm², 20.8A/mm² and 30.3A/mm², respectively (related to the copper surface). The total coolant volumetric flow rates of the complete electrical machine (i.e.

192 hollow conductors), converted from those of the 2 hollow conductors in the experiments, are 6.4L/min, 10.6L/min and 14.8L/min, respectively.

Due to the page limit, only the transient thermal results at 250A DC current and 0.11L/min flow rate are presented in this section. Fig. 9 compares the model-predicted and measured temperatures at coolant inlet (TP6 shown in Fig. 6), coolant outlet (TP7), front active winding (TP1/TP2), rear active winding (TP3/TP4), and rear end-winding (TP5).

The coolant inlet temperature in simulation is assumed to be the same as the measured in order to ensure consistency between the simulations and experiments using the same reference temperature as shown in Fig. 9 (a). The initial coolant temperature is 23.1°C.

It can also be seen that all the model-predicted temperatures at the coolant outlet, active winding and end-winding exhibit lower time constant, compared to those in the measurements. The mismatch between the prediction and measurement at TP1/TP2 is believed to be caused by the thermal mass effect of the clamps and thick electrical cables not being fully accounted. By correcting the thermal capacitances of the conductor elements, the agreement between the model-predicted and the measured transient temperature behaviors does improve. However, this problem does not exist in the machine windings as shown in Section IV and the correction is not justified.

It should be noted that the measured temperatures in the two conductor sides are slightly different, as shown in Fig. 9 (c) and (d). This may be caused by a number of factors. First, it is assumed that the coolant flow rates in the two sides are the same, but in reality they may differ slightly. The thermal couplers are glued to the conductors in the designated position, but the thickness of the glue and exact position may not be the same. Further, the measurement error may also contribute to the difference.

Table III lists the steady-state temperature errors of this proposed model. The measured temperatures in TP1/TP2 and TP3/TP4 refer to the mean temperatures of TP1/TP2 and TP3/TP4. It can be seen that the proposed model underestimates the front active winding (TP1/TP2) temperature by 12% with respect to the measurement. This is mainly due to the underestimate of the copper loss in the clamp which is adjacent to the TP1/TP2 sensor. This is because the calculation of the clamp resistance is based on the assumption of a uniform distribution of the current in the clamp while this assumption may underestimate the clamp resistance. Ideally, the current distribution in the clamp should be calculated by 3D FEA. However, this is not the main concern of this paper. A simplified analytic estimation of the clamp resistance is used here based on the clamp dimensions and conductivity. The copper loss per unit length of the cable before the clamp which is neglected in the model may also contribute to the deviation between the measured and predicted temperatures. However, these issues will not be present in machine windings with hollow conductors.

The steady-state temperature errors of the proposed model at TP3/TP4, TP5 and TP7 are within 2% compared to the measurements. This shows that the proposed thermal model of

a hollow conductor with direct cooling features can provide an accurate prediction of steady-state temperatures. There are also noticeable fluctuations in measured temperatures. This is because the pump system cannot maintain a constant flow rate in the experiments.

Fig. 10 shows the heat flow breakdown in the thermal simulation of the hollow conductor at 250A DC current and 0.11L/min flow rate. Table IV lists the heat power and heat energy at the end of this simulation. The simulation time duration is identical to that of measurement. It can be seen that at the end of the simulation, the majority (89.8% of heat power, 86.8% of heat energy) of the heat is dissipated to the coolant by the forced convection. Meanwhile 4.6% of heat power or 4.4% of heat energy is dissipated to the ambient by the natural convection and radiation. At the end of simulation, the heat power to heat up the copper drops to 5.6% rather than 0, due to the large thermal mass of the conductors, clamps and leads. On the other hand, the heat power to heat up coolant drops to 0 due to its negligible thermal mass.

TABLE III
TEMPERATURES AT 1600S WITH 250A DC CURRENT AND 0.11L/MIN FLOW RATE

Temperature sensor	Model prediction (°C)	Measurement (°C)	Error (%)
TP1/TP2	50.8	57.7	-12.0%
TP3/TP4	61.9	60.7	2.0%
TP5	61.6	61.2	0.7%
TP7	36.2	36.5	-0.8%

(a)

(b)

(c)
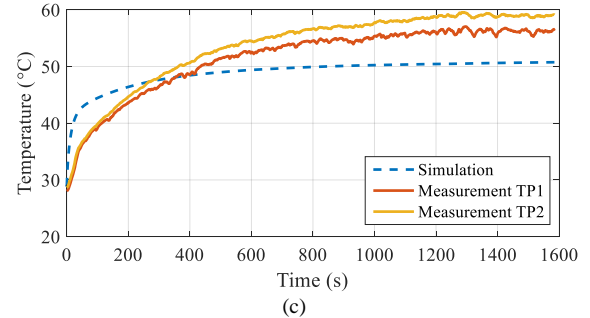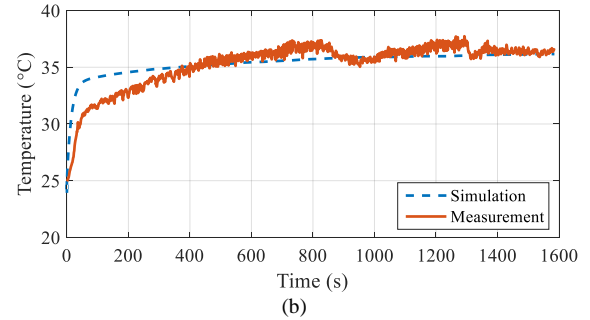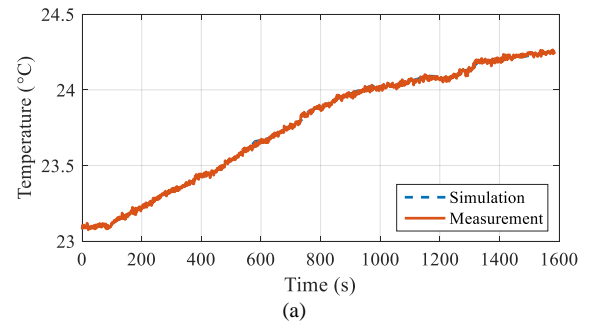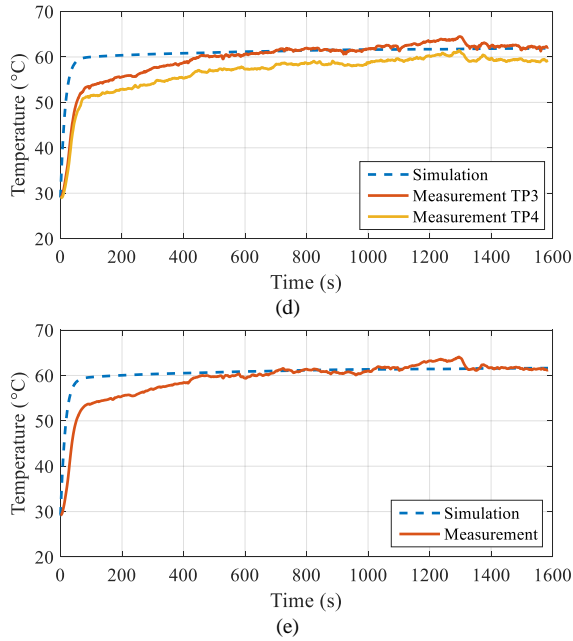
Fig. 9. Comparisons of the model-predicted and measured temperatures of the hollow conductor at 250A DC current (20.8A/mm^2 current density) and 0.11L/min flow rate. (a) Inlet (TP6). (b) Outlet (TP7). (c) Active winding – front (TP1/TP2). (d) Active winding – rear (TP3/TP4). (e) End-winding – rear (TP5).
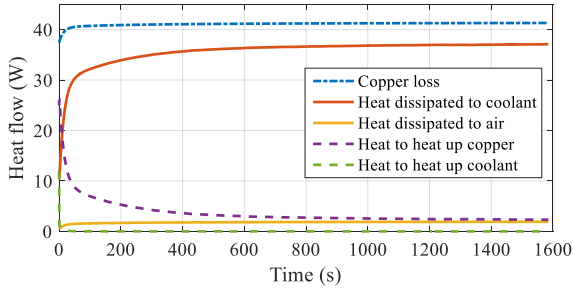
Fig. 10. Heat flow breakdown in the thermal simulation of the hollow conductor at 250A DC current (20.8A/mm^2 current density) and 0.11L/min flow rate.

TABLE IV
HEAT POWER AND HEAT ENERGY BREAKDOWN AT THE END OF THERMAL SIMULATION OF THE HOLLOW CONDUCTOR AT 250A DC CURRENT AND 0.11L/MIN FLOW RATE

Item	Heat power (W)	Ratio to total (%)	Energy (kJ)	Ratio to total (%)
Copper loss	41.30	-	65.17	-
Heat dissipated to coolant	37.10	89.83	56.57	86.80
Heat dissipated to air	1.90	4.60	2.86	4.39
Heat to heat up copper	2.30	5.57	5.72	8.78
Heat to heat up coolant	0.00	0.00	0.02	0.03

IV. APPLICATION

This section demonstrates the application of the proposed hollow conductor thermal model (in Fig. 4) in the thermal analysis of an IPM electrical machine with direct cooling features. Fig. 11 depicts the single tooth schematic of a 62.7 kW (130kW peak) electrical machine with hollow conductors. Each slot has 4 hollow conductors connected in the form of hairpin winding and 1 separator (for mechanical support) between conductors, as shown in Fig. 11. Coolant flows in each hollow

conductor in parallel via holes on the end-winding segment of the conductor. It should be noted that the dummy separator is only used to fit the slot area in an existing design, and not necessary in new designs with the cooling scheme. The hollow conductor is custom-made with standard extrusion process and coated with insulation.

The water cooling jacket is incorporated into the prototype machine in order to directly compare the heat dissipation performance to that of the direct cooling with hollow conductors. It should be noted that the periodicity in Fig. 11 does not applies to the water cooling channels. All the water cooling channels are axially connected in series with a zig-zag pattern, as shown in Fig. 12.

The experimental setup is shown in Fig. 13. The oil cooling circuit feeds the coolant which flows in the hollow conductors while the water circuit connects to the cooling jacket in the stator housing shown in Fig. 11. The cooling oil is fed into a sealed end-winding region and passes via a hole in the end-winding section of each conductor through the hollow region axially. The coolant is collected at the other end in a similar manner. Therefore, the cooling channels via the hollow conductors are connected in parallel. The details are covered in the patent [27].

The thermal measurements in this section are obtained at short circuit conditions. The prototype machine is driven by the load machine (shown in Fig. 13) at 3000r/min with 3-phase terminal short-circuit.

To demonstrate the benefits of the direct cooling scheme, the thermal experiments with two scenarios are performed, including (a) direct cooling only and (b) indirect cooling only.

In the direct cooling only scenario, the water pump is switched off while the oil pump drives Fragoltherm X80 through the hollow conductors at a total flow rate of 6.7L/min. The winding temperatures are measured by the thermocouples which are embedded adjacent to the conductors in the middle of the slots. To capture the possible uneven temperature distribution over all the slots due to potential uneven flow rate in the conductors, 1 type K thermocouple is placed in every 2 neighboring slots, as shown in Fig. 14.

In the indirect cooling only scenario, the oil pump is switched off while the water pump drives water circulation through the water cooling jacket at a flow rate of 12L/min.
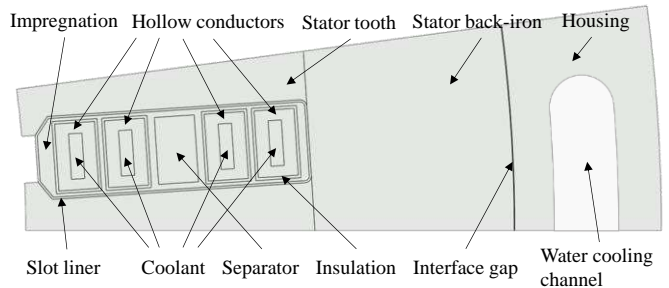
Fig. 11. Single tooth schematic of a 130kW electrical machine with hollow conductors, and water cooling jacket in stator housing.
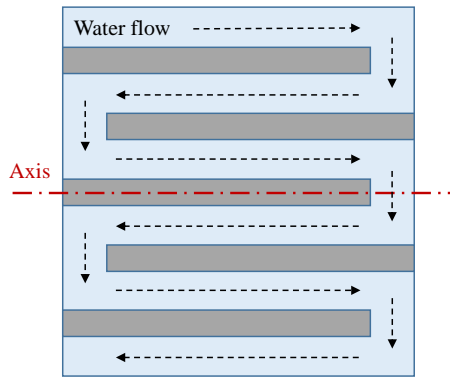
Fig. 12. Schematic of the water cooling channels and their connections.
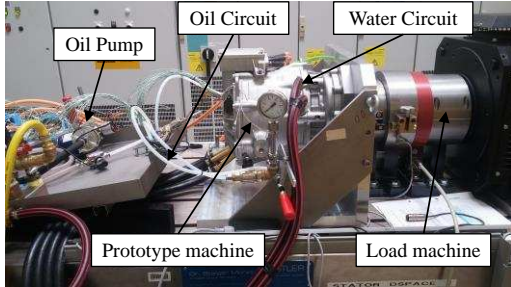
Fig. 13. Experimental setup for the thermal measurements of the prototype machine.
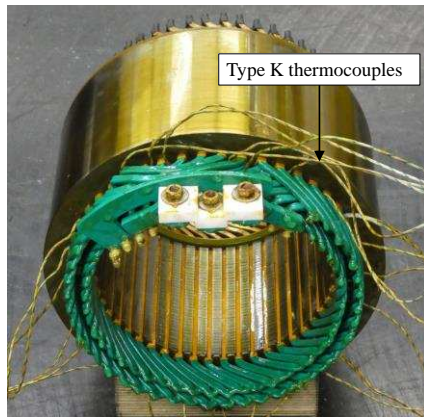
Fig. 14. Prototype machine stator and the thermocouples for winding temperature measurements.

Fig. 15 shows the model predicted mean winding temperature, the measured hotspot, coolspot and mean winding temperatures of the active windings for the direct cooling only and indirect cooling only scenarios. The 'measured mean' refers to the mean temperature of all the measured active winding temperatures from the thermocouples. The 'predicted mean' refers to the model-predicted mean temperature of the 4 hollow conductors in a slot.

The model used in this section is a Motor-CAD model with the modified thermal network of the windings according to those described in Section II. No hollow conductors with direct cooling features are available in the latest version of Motor-CAD. Additional coolant thermal nodes are added to model the non-uniform temperature distribution along axial direction. The equivalent thermal resistances between coolant and each cuboidal element are added to represent the direct cooling effects on the hollow conductors.

The model predicted temperatures in Fig. 15 are obtained

based on the measured machine losses as listed in Table V. The DC copper loss is calculated using the measured phase current and mean temperatures. The AC copper loss is calculated based on the FE-predicted ratio of AC to DC copper losses. The total machine loss is the measured mechanical power at terminal short circuit condition. The iron loss and mechanical loss are calculated by subtracting the total copper loss from the total machine loss.

From Fig. 15 (a), it can be seen that the measured hotspot in the active winding is 8.8°C (20%) higher than the coolspot in the direct cooling only scenario. This is mainly due to the uneven flow rates over various slots caused by the gravity. However, the predicted mean temperature (47.5°C) is only 2.1°C (4.1%) lower than the measured mean temperature (49.6°C) at the thermal steady-state, as listed in Table VI. The error in the transient waveforms is much less than that in the hollow conductor experiment shown in Fig. 9 in Section III.

From Fig. 15 (b), it can be observed that the measured hotspot in the active winding is 17.4°C (24.2%) higher than the coolspot in the indirect cooling scenario. This temperature difference is even higher than that in the direct cooling only scenario. This is because the water flows in the direction shown in Fig. 12 and thus the slots close to the outlet exhibits higher temperatures than those neighboring the inlet. However, the predicted mean temperature (80.3°C) is only 0.8°C (1%) higher than the measured mean temperature (79.5°C) at the thermal steady-state, as listed in Table VI.

It should be noted that the end-winding temperatures are measured at only a few locations and thus their mean temperatures are easily disturbed by the uneven flow rates, but are lower than those in the slots. Therefore, they are not presented in this paper.
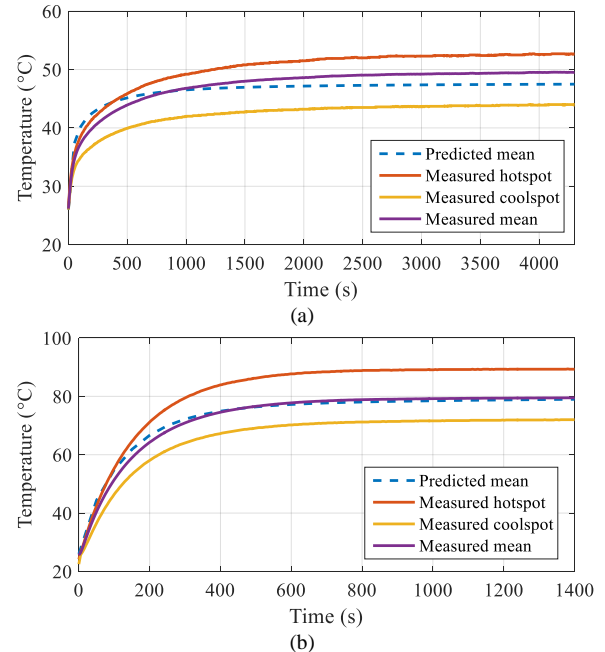
Fig. 15. Comparisons of the model-predicted and measured temperatures in the active windings under terminal short circuit conditions at 3000r/min. (a) Direct cooling only, 6.7L/min. (b) Indirect cooling only, 12L/min.

TABLE V
MEASURED MACHINE LOSS BREAKDOWN AT STEADY-STATE TERMINAL
SHORT CIRCUIT CONDITIONS AT 3000R/MIN

Item	Unit	Direct cooling only	Indirect cooling only
Phase current (RMS)	A	280	280
DC copper loss	W	1669.5	1813.7
Scaled AC copper loss	W	417.4	453.4
Total copper loss	W	2086.9	2267.1
Total machine loss	W	2410.0	2550.0
Iron loss and mechanical loss	W	323.1	282.9

TABLE VI
COMPARISON OF MEASURED AND PREDICTED WINDING TEMPERATURES AT
STEADY-STATE TERMINAL SHORT CIRCUIT CONDITIONS AT 3000R/MIN

Item	Unit	Direct cooling only	Indirect cooling only
Predicted mean	°C	47.5	80.3
Measured hotspot	°C	52.8	89.4
Measured coolspot	°C	44.0	72.0
Measured mean	°C	49.6	79.5
Error in prediction	%	-4.1%	1.1%

By comparing the measured winding temperatures at the direct cooling and indirect cooling scenarios, it can be seen that by using the direct cooling scheme with 6.7L/min flow rate, the reduction in the active winding mean temperature is approximately 30°C compared to the indirect cooling scheme with 12L/min flow rate. This can significantly increase the life time of the insulation and also reduces the risks of irreversible demagnetization of magnets. Alternatively, considerably higher power density could be achieved with optimized design.

It should be noted that the prototype is built for the tests and validation purpose. Once the proposed cooling scheme has been tested and validated, the machine can be optimized with very significant weight and size reduction.

V. CONCLUSION

This paper has derived and validated a computationally efficient thermal model of hollow conductors with direct cooling features, considering temperature distributions over 3D thermal network, the internal heat generation, the fluid dynamics and the enthalpy carried by coolant. Compared to CFD analysis, the proposed thermal model is much more computationally efficient, and thus can be incorporated into design optimization process or electro-thermal simulations of the electric drive over a driving cycle or mission profile.

The proposed thermal model is applied to the thermal analysis of a 62.7 kW electrical machine with both direct cooling and indirect cooling features. By using the direct cooling scheme, significant winding temperature drop can be observed. This indicates that the direct cooling configuration with hollow conductors can considerably increase the life time of the machine or allow for significant improvements in torque density.

REFERENCES

[1] M. Popescu, D. A. Staton, A. Boglietti, A. Cavagnino, D. Hawkins, and J. Goss, "Modern Heat Extraction Systems for Power Traction Machines—A Review," IEEE Transactions on Industry Applications, vol. 52, pp. 2167-2175, 2016.

[2] L. Mingda, L. Yingjie, D. Hao, and B. Sarlioglu, "Thermal management and cooling of windings in electrical machines for electric vehicle and traction application," in 2017 IEEE Transportation Electrification Conference and Expo (ITEC), 2017, pp. 668-673.

[3] A. Tüysüz, M. Steichen, C. Zwyssig, and J. W. Kolar, "Advanced cooling concepts for ultra-high-speed machines," in 2015 9th International Conference on Power Electronics and ECCE Asia (ICPE-ECCE Asia), 2015, pp. 2194-2202.

[4] G. Karimi-Moghaddam, R. D. Gould, S. Bhattacharya, and D. D. Tremelling, "Thermomagnetic liquid cooling: A novel electric machine thermal management solution," in 2014 IEEE Energy Conversion Congress and Exposition (ECCE), 2014, pp. 1482-1489.

[5] D. Tanguy, S. Harmand, J. Pelle, and R. Yu, "Experimental study of oil cooling systems for electric motors," Applied Thermal Engineering, vol. 71, p. 607, 2014/10/05/ 2014.

[6] I. A. Metwally and A. A. A. Rahim, "Flow electrification phenomenon in forced air-cooled rotating electric machines," IEEE Transactions on Dielectrics and Electrical Insulation, vol. 5, pp. 966-971, 1998.

[7] X. Sun and M. Cheng, "Thermal Analysis and Cooling System Design of Dual Mechanical Port Machine for Wind Power Application," IEEE Transactions on Industrial Electronics, vol. 60, pp. 1724-1733, 2013.

[8] S. Nategh, O. Wallmark, M. Leksell, and S. Zhao, "Thermal Analysis of a PMaSRM Using Partial FEA and Lumped Parameter Modeling," IEEE Transactions on Energy Conversion, vol. 27, pp. 477-488, 2012.

[9] C. Kral, A. Haumer, and T. Bauml, "Thermal Model and Behavior of a Totally-Enclosed-Water-Cooled Squirrel-Cage Induction Machine for Traction Applications," IEEE Transactions on Industrial Electronics, vol. 55, pp. 3555-3565, 2008.

[10] G. B. Sugden, "Oil-cooled a.c. generators for aircraft -- present trends," Students' Quarterly Journal, vol. 40, pp. 128-133, 1970.

[11] K. Nakamura and Y. Hayashi, "Motor Cooling System," US Patent US4959570A, 1990.

[12] Z. Li, J. Guo, D. Fu, G. Gu, and B. Xiong, "Research on heat transfer of spraying evaporative cooling technique for large electrical machine," in 2009 International Conference on Electrical Machines and Systems, 2009, pp. 1-4.

[13] P. Arumugam, C. Gerada, S. Bozhko, H. Zhang, W. Fernando, A. La Rocca, et al., "Permanent Magnet Starter-Generator for Aircraft Application," SAE Technical Paper 2014-01-2157, 2014.

[14] Z. Xu, A. L. Rocca, P. Arumugam, S. J. Pickering, C. Gerada, S. Bozhko, et al., "A semi-flooded cooling for a high speed machine: Concept, design and practice of an oil sleeve," in IECON 2017 - 43rd Annual Conference of the IEEE Industrial Electronics Society, 2017, pp. 8557-8562.

[15] Z. Huang, S. Nategh, V. Lassila, M. Alaküla, and J. Yuan, "Direct oil cooling of traction motors in hybrid drives," in 2012 IEEE International Electric Vehicle Conference, 2012, pp. 1-8.

[16] R. Camilleri, D. A. Howey, and M. D. McCulloch, "Predicting the Temperature and Flow Distribution in a Direct Oil-Cooled Electrical Machine With Segmented Stator," IEEE Transactions on Industrial Electronics, vol. 63, pp. 82-91, 2016.

[17] R. Camilleri, P. Beard, D. A. Howey, and M. D. McCulloch, "Prediction and Measurement of the Heat Transfer Coefficient in a Direct Oil-Cooled Electrical Machine With Segmented Stator," IEEE Transactions on Industrial Electronics, vol. 65, pp. 94-102, 2018.

[18] P. M. Lindh, I. Petrov, R. S. Semken, M. Niemelä, J. J. Pyrhönen, L. Aarniovuori, et al., "Direct Liquid Cooling in Low-Power Electrical Machines: Proof-of-Concept," IEEE Transactions on Energy Conversion, vol. 31, pp. 1257-1266, 2016.

[19] P. Lindh, I. Petrov, A. Jaatinen-Värri, A. Grönman, M. Martinez-Iturralde, M. Satrústegui, et al., "Direct Liquid Cooling Method Verified With an Axial-Flux Permanent-Magnet Traction Machine Prototype," IEEE Transactions on Industrial Electronics, vol. 64, pp. 6086-6095, 2017.

[20] A. Boglietti, A. Cavagnino, D. Staton, M. Shanel, M. Mueller, and C. Mejuto, "Evolution and Modern Approaches for Thermal Analysis of Electrical Machines," IEEE Transactions on Industrial Electronics, vol. 56, pp. 871-882, 2009.

[21] S. A. Semidey and J. R. Mayor, "Experimentation of an Electric Machine Technology Demonstrator Incorporating Direct Winding Heat Exchangers," IEEE Transactions on Industrial Electronics, vol. 61, pp. 5771-5778, 2014.

[22] M. Schiefer and M. Doppelbauer, "Indirect slot cooling for high-power-density machines with concentrated winding," in 2015 IEEE International Electric Machines & Drives Conference (IEMDC), 2015, pp. 1820-1825.

[23] A. W. V. Madonna, P. Giangrande, G. Serra, C. Gerada, M. Galea, "Improved thermal management and analysis for stator end-windings of electrical machines," IEEE Trans. Industrial Electronics, early access.

[24] R. Wrobel and P. H. Mellor, "A General Cuboidal Element for Three-Dimensional Thermal Modelling," IEEE Transactions on Magnetics, vol. 46, pp. 3197-3200, 2010.

[25] G. Nellis and S. Klein, Heat Transfer: Cambridge University Press, 2009.

[26] P. Wibulswas, "Laminar Flow Heat Transfer in Non-Circular Ducts," Ph.D Thesis, University of London, London, 1966.

[27] D. Diehl, M. Klöpzig, H. Schmidt, A. Schröter, A. Spagnolo, and M. Wilke, "Stator mit Wicklungskühlung und elektrische Maschine," Deutschland Patent DE 10 2017 204 472 A1, 2018.

Xiao Chen (S'13-M'16) received B.Eng. and M.Eng. degrees in electrical engineering from Harbin Institute of Technology, Weihai and Harbin, China, in 2009 and 2011, respectively, and Ph.D degree in electrical engineering from The University of Sheffield, Sheffield, UK, in 2015. He is currently a Research Associate in the Department of Electronic and Electrical Engineering, The University of Sheffield, UK. His current research interests include the modeling, design and analysis of permanent-magnet synchronous machines for traction applications.

Jiabin Wang (S'94–A'96–M'01–SM'03) received the B.Eng. and M.Eng. degrees from Jiangsu University of Science and Technology, Zhenjiang, China, in 1982 and 1986, respectively, and the Ph.D. degree from the University of East London, London, U.K., in 1996, all in electrical and electronic engineering.

Currently, he is a Professor in Electrical Engineering at the University of Sheffield, Sheffield, U.K. From 1986 to 1991, he was with the Department of Electrical Engineering at Jiangsu University of Science and Technology, where he was appointed a Lecturer in 1987 and an Associated Professor in 1990. He was a Postdoctoral Research Associate at the University of Sheffield, Sheffield, U.K., from 1996 to 1997, and a Senior Lecturer at the University of East London from 1998 to 2001. His research interests range from motion control and electromechanical energy conversion to electric drives for applications in automotive, renewable energy, household appliances and aerospace sectors.

He is a fellow of the IET and a senior member of IEEE.

Antonio Griffo (M'13) received the M.Sc. degree in electronic engineering and the Ph.D. degree in electrical engineering from the University of Napoli "Federico II," Naples, Italy, in 2003 and 2007, respectively. From 2007 to 2013, he was a Research Associate with The University of Sheffield, Sheffield, U.K., and the University of Bristol, Bristol, U.K. He is currently a Senior Lecturer in the Department of Electronic and Electrical Engineering, The University of Sheffield. His research interests include modeling, control, and condition monitoring of electric power systems, power electronics converters, and electrical motor drives for renewable energy, automotive, and aerospace applications.

Dr. Ing Aristide Spagnolo earned the Master Degree in Electrical engineering in 2006 and the Ph.D. degree in 2011 at the University of Padua, Italy.

Since 2012 he is working at Siemens Corporate Technology in Erlangen, Germany, on different R&D projects in the field of electrical machines and drive technology. He is author and co-author of several international publications.